Summer August 13, 2018

Synthesis and characterization of Zinc/Chitosan-Folic acid complex

Subhani Bandara, *Prairie View A&M University*
Codi-anne Carnegie
Chevaun Johnson
Feyisayo Akindoju
Ebonee Williams, et al.

Heliyon

Received:
12 October 2017
Revised:
19 June 2018
Accepted:
13 August 2018

Cite as: Subhani Bandara, Codi-anne Carnegie, Chevaun Johnson, Feyisayo Akindoju, Ebonee Williams, Julia M. Swaby, Aderemi Oki, Laura E. Carson. Synthesis and characterization of Zinc/Chitosan-Folic acid complex. Heliyon 4 (2018) e00737.
doi: 10.1016/j.heliyon.2018.e00737

Synthesis and characterization of Zinc/Chitosan-Folic acid complex

Subhani Bandara [a], Codi-anne Carnegie [a], Chevaun Johnson [a], Feyisayo Akindoju [a], Ebonee Williams [a], Julia M. Swaby [a], Aderemi Oki [b], Laura E. Carson [a,*]

[a] *Cooperative Agricultural Research Center, Prairie View A&M University, Prairie View, TX 77446, USA*

[b] *Department of Chemistry, Prairie View A&M University, Prairie View, TX 77446, USA*

[*] Corresponding author.

E-mail address: lecarson@pvamu.edu (L.E. Carson).

Abstract

Therapeutic drug delivery systems using polymeric materials is an emerging field of research. However, the use of certain polymers has gained much-needed attention by the researchers due to their low toxic nature. In recent years, chitosan has gained popularity as a potential biodegradable polymer that can be used as a component in drug delivery systems. In this study, we synthesized a chitosan derivative that is composed of both folic acid and zinc and may serve as a viable component of a drug delivery system. The results of Fourier Transform Infrared Spectroscopy (FTIR), solid-state ^{13}C Nuclear Magnetic Resonance Spectroscopy (NMR) and UV-visible Spectroscopy demonstrated a substantial difference between chitosan and ZnS/Chitosan-Folic acid derivative. The results were also confirmed using Thermogravimetric Analysis (TGA) and Scanning Electron Microscopy/Energy Dispersive X-ray Spectroscopy (SEM-EDS) techniques. The average particle size of the ZnS/Chitosan-Folic acid system was measured to be 463.67 $\pm$ 5.76 nm, showing that the product is within the nano-size range.

Keyword: Materials science

https://doi.org/10.1016/j.heliyon.2018.e00737

1. Introduction

Nano-based technology is widely used in a variety of fields including agriculture and biomedicine (Cho et al., 2010; Parveen et al., 2012). Nano-sized materials have the ability to penetrate the cell membrane and thus interact with intracellular organelles in order to deliver the necessary treatment to specific abnormal cells (Hughes, 2005). Hence, the research herein is focused on developing a polymer-based delivery system that can be used to selectively target defective cells, while not affecting healthy cells. Chitosan (CS), a copolymer composed of D-glucosamine and N-acetylglucosamine, has been shown to have potential use in food and agricultural industry and medical fields (Li et al., 1992). The potential use of chitosan is aligned with its high biocompatibility, its nontoxicity, and its environmental friendly nature. It has a highly functional backbone, which makes it ideal for encapsulating suitable entities, and has shown promising possibilities of protecting conjugated quantum dots composite materials (Lv et al., 2013). Further investigations have shown that chemical modification of chitosan leads to the enhancement of its properties and supports the development of viable, efficient delivery systems. That is, the chemical modification of chitosan provides a level of control at the interface of the modified chitosan derivatives and tends to increase its ability to deliver the necessary component to specific cells (Prabaharan, 2008). Other polymer based drug carriers like polyethylene glycol have also been investigated, but require additional organic components to be systematically functional (Colangelo et al., 2013). In addition, the properties such as charge and size are important considerations when designing a drug delivery system. The cationic nature of chitosan, facilitates interactions with negatively charged cell membrane, allowing easy intake by cells via endocytosis (Mansouri et al., 2006; Park et al., 2010). Also, the positive charge on chitosan allows the formation of complexes with negatively charged molecules such as DNA, proteins and peptides, providing means of formulating therapeutic delivery systems. The size requirement of the nanoparticles can vary based on the target organ and pathological features. Although, nanoparticles size can be distributed in a wide range ($<$1um), particles below 200 nm are of higher demand due to ease of reaching the target sites (Singh and Lillard, 2009). Chitosan-based nanoparticles that are conjugated with small molecules are shown to fall in this required size range, making them good candidates for delivery systems (Gan et al., 2005; Vaezifar et al., 2013).

Another important component of a targeted delivery system is the use of naturally occurring trace metals like zinc (Zn), copper (Cu), manganese (Mn) and iron (Fe) (Ndagi et al., 2017). Zinc is the second most abundant trace metal found in eukaryotic organisms and is essential for basic biological functions (Coleman, 1992). The properties of zinc are being heavily studied since its recent approval by the US Food and Drug Administration (FDA) in 2015 (Bakrudeen et al., 2015). Photo physical studies have suggested that zinc quantum dots have potential therapeutic

https://doi.org/10.1016/j.heliyon.2018.e00737

applications due to their ability to absorb energy in the near infrared region (Al-Adilee et al., 2016; Plaetzer et al., 2009). This indicates the usefulness of Zn in a targeted delivery system, in destroying the defective cells while maintaining the integrity of healthy cells.

Yet another important part of a delivery system is its ability to target well-known receptors or cells. Folic acid (FA) is a form of vitamin B, and a more stable oxidized folate ion form is primarily found in supplements and fortified food (Crider et al., 2011). Certain types of cancer cells are known to overexpress folic acid receptors, as they require FA for their functioning (Luong et al., 2017; Nickerson and Webb, 1956). Hence, FA can be used to target these cells, as they are capable of uptaking it via receptor-mediated endocytosis. Folic acid-linked nanoparticle components may represent the type of carrier system that can serve dual purposes to include inhibiting cell growth in microbes and cancer. In this study, a nano-sized delivery system was synthesized using chitosan, zinc and folic acid and is reported herein.

2. Materials and methods

2.1. Chemicals

Low molecular weight chitosan (50−190 kDa) with the degree of deacetylation 75−85%, zinc chloride (reagent grade, $\geq$ 98%) and thiourea (ACS grade, 99%) were purchased from Sigma-Aldrich, USA (St-Louis, MO). Potassium persulfate (99.9% trace metals) and tetrahydrofuran (THF) (99.8%) were purchased from Acros Organics (New Jersey, USA). Ethanol and glacial acetic acid were purchased from Fisher Scientific (Hampton, NH). The proposed synthesis scheme is shown in Fig. 1.

2.2. Material characterizations

Fourier transform infrared (FTIR) analysis was conducted on the chitosan derivatives from 4000 cm^{-1} to 600 cm^{-1} using IdentifyIR Portable FTIR Spectrometer (Betatek Inc., Canada). The samples were directly applied onto the diamond crystal and recorded spectra using the Attenuated Total Reflection (ATR) method. The spectrophotometric studies were carried out using SPECTROstar Nano spectrophotometer (BMG LABTECH, Germany). The samples were dissolved in 1% acetic acid ($\sim$0.2 mg/ml) and the measurements were taken using Plastic UV cuvettes (BrandTec) with 10 mm optical path length with 1% acetic acid as the reference. The particle size, polydispersity index (PDI) and zeta potential of the samples dissolved in 1% acetic acid (dispersant refractive index = 1.33) was measured using Zetasizer nano ZS (Malvern Instruments, UK) at 25 °C. The size was measured by the Zetasizer using dynamic light scattering, and the measurement was repeated three times. Zeta potential was measured using the electrophoretic mobility of the particles, and the measurements were repeated three times with a minimum of 12

https://doi.org/10.1016/j.heliyon.2018.e00737

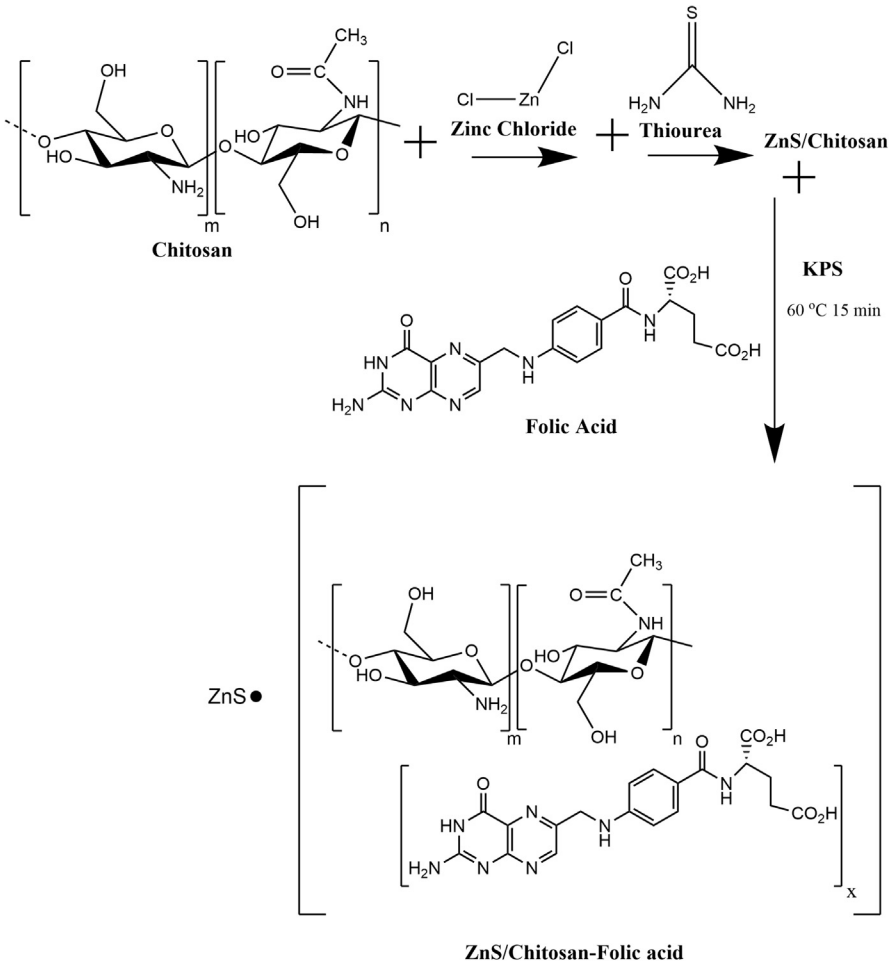

Fig. 1. Proposed schematic diagram of the preparation of ZnS/Chitosan-Folic acid.

runs for each measurement. Thermal analyses were performed using the TGA Q500-0456 (TA Instruments-Waters LLC, Delaware, USA) at 20 °C/min heating rate under nitrogen atmosphere from 25 °C to 1000 °C to assess the thermal stability. Typically, the weight loss percentage and residual percentage were calculated using the Universal Analysis 2000 system. SEM-EDS, and solid-state ^{13}C NMR experiments were carried out at Texas A&M University, College Station. SEM and EDS analyses were conducted with JEOL JSM-7500F Field Emission Scanning Electron microscope (JEOL, Tokyo, Japan) to characterize the shape and microstructure of the samples after sputter coating with Pt. Solid-state ^{13}C Cross-Polarization NMR spectra were collected on a Bruker Avance 400 MHz spectrometer (Bruker BioSpin, USA) using a 7 mm MAS probe at TAMU, College Station Texas.

2.3. Synthesis of ZnS/Chitosan

Chitosan was purified using methods reported in the literature (Carson et al., 2009). During the purification, chitosan was dissolved in 1% acetic acid and filtered to

https://doi.org/10.1016/j.heliyon.2018.e00737

remove residues. Then 2 M sodium hydroxide was added to the solution and stirred for 30 min. Afterwards, excess sodium hydroxide was removed, and the filtrate was washed with distilled water until neutral pH was achieved. Then, the sample was freeze-dried using VirTis BenchTop Pro with Omnitronics freeze dryer (SP Scientific, NY USA) for 48 h. Afterwards purified chitosan was used for the synthesis of ZnS/Chitosan, using thiourea as the source of sulfur for the formation of zinc sulfide nanoparticles (Ghosh et al., 2006). During this synthesis 3.0 mmol of purified chitosan was added to 200 mL of distilled water and sonicated for 30 min using 130 watt Vibra Cell Ultrasonic processor (Sonics & Materials, Inc., USA). Then a solution of zinc chloride (0.804 mmol in 50 ml distilled water) was added drop wise to the chitosan solution using a transfer pipette and stirred for 30 min to obtain a homogenous solution. Then, the round bottom flask containing the solution was connected to a Liebig condenser and placed in an oil bath at 135−137 °C. Afterwards, thiourea solution (0.0901 mmol in 50 mL of distilled water) was added drop wise through the Liebig condenser and allowed to react for 4 h.

After 4 h the mixture was cooled, the sample was centrifuged at 5000 rpm (3550 g) for 5 min at room temperature, and the supernatant was removed. Ethanol (70%) of equal volume was added to wash the solid sample before drying for 48 h at 60 °C.

2.4. Synthesis of ZnS/Chitosan-Folic acid

After chitosan-zinc sulfide sample was fully dried, the sample was dissolved in 100 mL of 1% acetic acid. The solution was transferred to a round bottom flask and 5.43 mmol folic acid was added and gently stirred for 3 min. The mixture was then set into an oil bath at 60 °C and 3.7 mmol Potassium persulfate (KPS) was added to the reaction mixture as a free radical initiator to facilitate further degradation of chitosan and incorporation of folic acid into the matrix (Hsu et al., 2002). The viscosity of the solution was observed to be reduced significantly after the reaction with KPS indicating that degradation of the polymer has occurred. After 15 min, 100 mL THF was added to the solution to terminate the reaction. Then, layered cheesecloth was used to quickly filter the sample as cheesecloth is compatible with the chemicals used during the synthesis (specifically THF) and was readily available in the lab. The filtrate was dialyzed (Mw cut off 10,000) against distilled water for two days at room temperature. The resulting sample was freeze-dried using VirTis BenchTop Pro with Omnitronics freeze dryer (SP Scientific, NY USA) for 48 h.

3. Results and discussion

3.1. FTIR studies

The FTIR spectra of chitosan derivatives (Fig. 2) show peaks that are inherent to specific functional groups. Specifically, the peak at 3337 cm^{-1} in chitosan indicated the

https://doi.org/10.1016/j.heliyon.2018.e00737

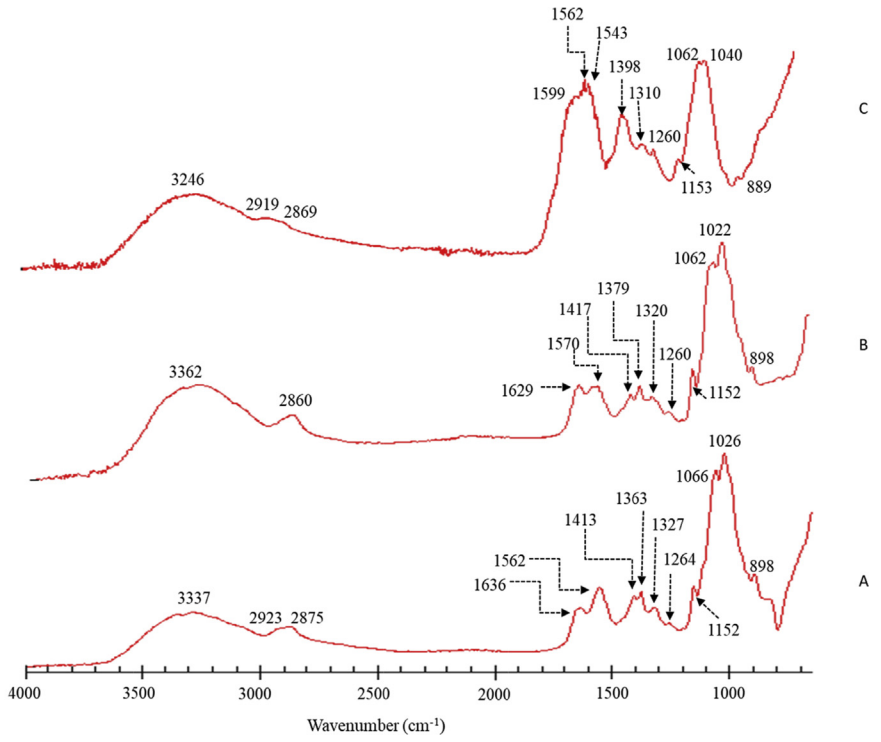

Fig. 2. Fourier transform infrared spectra of (A) chitosan (B) ZnS/Chitosan and (C) ZnS/Chitosan-Folic acid.

presence of O-H and an N-H stretching vibrations. Peaks observed at 2923 cm^{-1} and 2875 cm^{-1} are attributed to C-H stretching vibrations of chitosan as reported in the literature (Xiao et al., 2015; Khoza and Nyokong, 2015). The peak at 1636 cm^{-1} was assigned to C=O stretching vibrations of amide group (amide I) derived from the residues that are not deacetylated in chitosan. Then, the peak at 1562 cm^{-1} (amide II) was due to N-H bending vibrations from both amide group and the deacetylated primary amine group present in chitosan (Bujňáková et al., 2017b). Also, the C-H vibrations due to the methyl group of amide can be assigned to 1363 cm^{-1} peak in the spectrum. Additionally, O-H and C-H vibrations of chitosan ring structure are indicated by the peaks at 1413 cm^{-1} and 1327 cm^{-1} respectively. The peak at 1264 cm^{-1} represents the C-N stretching and N-H bending vibrations of the amide group and the peaks observed in the range of 1155 cm^{-1} − 800 cm^{-1} are known to arise from C-O stretching vibrations in chitosan (Bujňáková et al., 2017b).

After deposition of zinc on chitosan, a slight shift of peaks was detected with N-H stretching vibrations at 3362 cm^{-1}, C-H stretching at 2860 cm^{-1} and amide I and II peaks at 1629 cm^{-1} and 1570 cm^{-1} respectively. From the peaks in the range of 1400 cm^{-1} − 800 cm^{-1}, a noticeable shift was observed for the C-H vibration of amide methyl group at 1379 cm^{-1}. These minor shifting in the peak positions are believed to be due to interactions between chitosan and zinc (Liu et al., 2001; Ryu et al., 2010). The product synthesized from the reaction of chitosan, zinc

https://doi.org/10.1016/j.heliyon.2018.e00737

chloride, and folic acid showed peaks within the range 3200 cm^{-1}- 3000 cm^{-1} attributed to N-H and O-H stretching. Also, in ZnS/CS-FA shifts were observed in comparison to chitosan and ZnS/Chitosan samples with amide I peak at 1599 cm^{-1}, methyl group C-H vibration at 1398 cm^{-1}, ring C-H vibrations at 1310 cm^{-1} and C-O stretching vibrations at 1040 cm^{-1} and 898 cm^{-1} indicating that a change has occurred after the reaction with folic acid. A new peak was observed at 1543 cm^{-1}, in the region of N-H bending vibrations and can be assigned to the additional N-H groups coming from folic acid. The peak ~ 1400 cm^{-1} due to O-H ring vibrations was not observed in the ZnS/CS-FA spectrum. This peak can be masked due to the peak at 1398 cm^{-1} from C-H vibration, which was shifted from the related peaks observed for CS and ZnS/CS at 1363 cm^{-1} and 1379 cm^{-1}, respectively. These changes further indicated the incorporation of folic acid to chitosan. It is worth noting that the ester formation was minimal in the sample due to the absence of peaks in the range of 1735−1750 cm^{-1}.

3.2. NMR

^{13}C NMR data (Fig. 3) provided evidence to show that folic acid may be attached to chitosan. Carbon assignments for chitosan in Fig. 3 were as follows: $\delta_{102.1}$ for C-1; $\delta_{54.4}$ for C-2; $\delta_{72.4}$ for C-3 and C-5 overlaps; $\delta_{79.4}$ for C-4 and $\delta_{58.1}$ for C-6. Due to the presence of residual acetyl groups in chitosan, peaks were observed at $\delta_{171.1}$ and $\delta_{20.7,}$ which were attributed to C_a and C_b, respectively, as seen in the literature (Saito et al., 1987). While similar spectrum was observed for chitosan and ZnS/CS, the ^{13}C NMR for ZnS/CS-FA spectrum shows additional peaks within the range of $\delta_{120\ -\ 160,}$ which can be assigned to the ring structures (C4' − C13') of folic acid. Other assignments in the range of $\delta_{20\ -\ 40}$ can be attributed to C15' − C17'

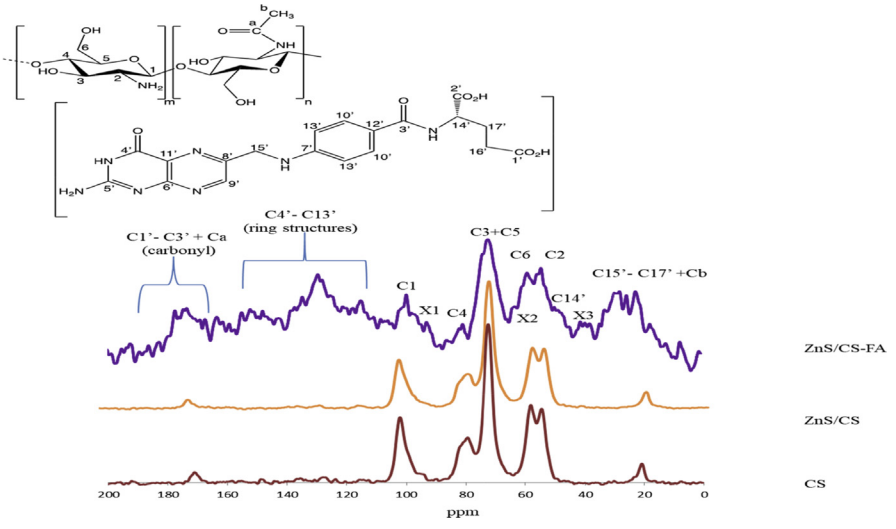

Fig. 3. Solid State ^{13}C NMR spectra of chitosan (red), ZnS/Chitosan (orange) and ZnS/Chitosan- Folic acid (purple).

https://doi.org/10.1016/j.heliyon.2018.e00737

of folic acid and the small peak around δ_{49} can be assigned to C-14 of folic acid. The peaks around $\delta_{170\ -\ 180}$ can occur due to the carbonyl groups in folic acid (C1' − C3'). Additionally, the remaining residual acetyl groups of chitosan can contribute to the peaks around δ_{170} and δ_{20}. Thus, the peaks observed indicate the presence of both chitosan and folic acid in the sample. According to these results, it can be seen that folic acid was incorporated into the chitosan matrix. But, indications of possible bond formations between chitosan and folic acid can be masked due to less defined, overlapping signals of the spectrum. Also, folic acid contains various possible sites which can react with the free radical end (C1) of the chitosan generated by the reaction with KPS (Ganji and Abdekhodaie, 2008). Hence, the additional small peaks observed in the spectrum that are marked as X1 ($\delta_{100\ -\ 93}$), X2 ($\delta_{62.0}$), X3 ($\delta_{37\ -\ 41}$) can be indications of attachment of folic acid to chitosan at certain sites. In addition, folic acid being an excellent free radical scavenger (Joshi et al., 2001), could neutralize the generated free radicals leading to low levels of conjugation with chitosan. Hence, it is believed that folic acid is mainly complexed with chitosan via hydrogen bonding and van der Waals interactions.

3.3. UV-Visible spectroscopy

The UV-Vis absorbance spectra of purified chitosan, ZnS/CS, and ZnS/CS-FA solutions are shown in Fig. 4. As observed in the literature, chitosan sample did not show much absorbance in the wavelength range from 220 nm−800 nm due to lack of conjugated double bonds in the structure (Bujňáková et al., 2017b). In ZnS/CS sample, the peak observed at 228 nm corresponds to chitosan which is red shifted compared to pure chitosan (~208 nm), indicating interactions between chitosan and ZnS. Then the broad peak observed from 270 nm−330 nm for ZnS/CS can be attributed to ZnS nanocrystals, which is blue shifted in comparison with bulk ZnS (343 nm) (Bujňáková et al., 2017a; Ghosh et al., 2006). On the other

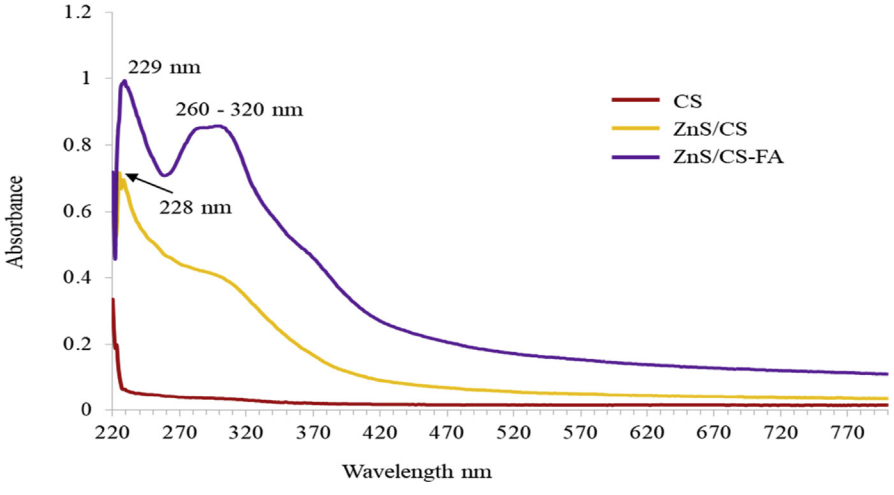

Fig. 4. UV-Vis absorbance spectra of chitosan (red), ZnS/CS (yellow) and ZnS/CS-FA (purple).

https://doi.org/10.1016/j.heliyon.2018.e00737

hand, red shifted chitosan peak was also observed for ZnS/CS-FA sample at 229 nm. Furthermore, ZnS/CS-FA showed a well distinguishable absorption peak in the range of 260 nm−320 nm which indicates the presence of folic acid as seen in the literature (Pujana et al., 2014). Pure folic acid solutions were reported to have absorption peaks at 255.5 nm, 283.0 nm and 365.5 nm wavelengths (Ribeiro et al., 2016) and the differences observed in the spectrum of ZnS/CS-FA compared to that of pure folic acid solutions can be attributed to the interactions between ZnS/CS and folic acid.

3.4. Thermal analysis

Thermal history of the samples was determined using Thermogravimetric Analysis (TGA), and the results were analyzed using Universal Analysis 2000 software (Fig. 5). For all chitosan derivatives, degradation began near 50 °C as observed in the graphs. The weight change in this region can be due to loss of moisture from the samples in agreement with the literature (Bwatanglang et al., 2016). Consistent with previous studies, a sharp degradation occurred between 250 °C−350 °C for all the samples, and is attributed to the loss of CO_2 (Bwatanglang et al., 2016). The thermal decomposition curve of ZnS/CS-FA closely followed the curve of ZnS/CS up to ~450 °C and showed faster decomposition from 450 °C−1000 °C. This broad decomposition range may indicate decarboxylation occurring with loss of CO_2 due to additional COO^- groups introduced from folic acid. Noticeably in the thermal history, very little of the ZnS/Chitosan-Folic acid derivative (weight 1.98%) remained at 1000 °C and showed that incorporation of folic acid may reduce the thermal stability of Zn coated chitosan at higher temperatures. This type of lowered stability was also observed for polyethylene glycol based nano sheets after modifying with folic acid (Vimala et al., 2017). When 5% and 10% weight losses for each derivative were compared (Table 1), the folic acid derivative exhibited similar

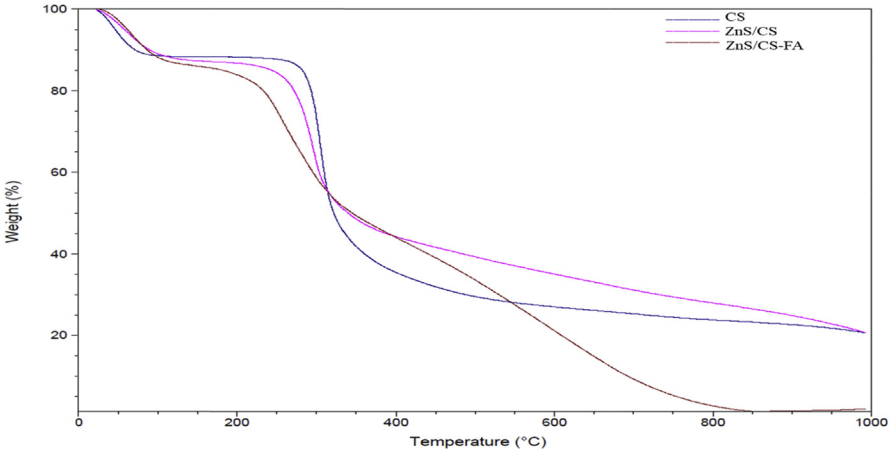

Fig. 5. Thermogravimetric analyses (TGA) curves of chitosan, ZnS/Chitosan, and ZnS/Chitosan-Folic acid samples.

https://doi.org/10.1016/j.heliyon.2018.e00737

Table 1. Thermal behavior of chitosan (CS) and its derivatives analyzed using Universal Analysis 2000 software.

Name of Sample	5% Weight Loss	10% Weight Loss	20% Weight Loss	Residue %	First derivative weight loss Temperature
CS	46.44 °C	71.47 °C	293.27 °C	20.66%	305.06 °C
ZnS/CS	58.00 °C	89.58 °C	272.09 °C	25.78%	295.60 °C
ZnS/CS-FA	61.55 °C	86.44 °C	233.13 °C	1.98%	256.31 °C

weight loss temperatures to ZnS/CS as seen in earlier studies (Bwatanglang et al., 2016). But 20% weight loss temperature was lowered with the addition of ZnS and folic acid to chitosan. The first derivative weight loss temperature is the temperature at which the greatest change occurs for each sample, and this value was observed to be shifted downwards with the incorporation of folic acid. The thermal behavior seen for the degradation of the Zn/Chitosan-Folic acid is aligned with similar studies and indicate that the product had considerable stability in the temperature range up to ~450 °C (Bwatanglang et al., 2016; Vimala et al., 2017).

3.5. SEM-EDS studies

According to the SEM images of chitosan and its derivatives (Fig. 6), purified chitosan was wisp-like and porous (Fig. 6a) while ZnS/CS appeared rough with an uneven surface (Fig. 6b). The appearances of both are aligned with results from previous studies (Ivan'kova et al., 2016; Mende et al., 2016). After the reaction with folic acid, the surface of the sample showed bead-like structures (Fig. 6 c) indicating a change has occurred. Further evidence for the presence of ZnS in ZnS/CS and ZnS/CS-FA was seen in EDS studies and is represented in Fig. 7b and 7c, respectively. In ZnS/CS sample, Zn is observed along with Cl atoms while in ZnS/CS-FA samples, Cl is not observed. The presence of Cl in ZnS/CS could indicate insufficient washing of the samples after reacting with $ZnCl_2$. However, the absence of Cl in the ZnS/CS-FA samples shows that Cl is removed during the downstream processing of the ZnS/CS samples. In addition, the color of chitosan solution changed from white to off-white after reacting with $ZnCl_2$. Then, a color change

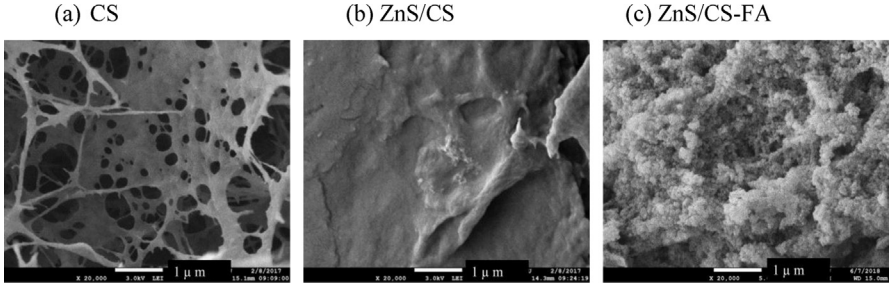

Fig. 6. SEM images of (a) Chitosan, (b) ZnS/Chitosan, (c) ZnS/Chitosan-Folic acid.

https://doi.org/10.1016/j.heliyon.2018.e00737

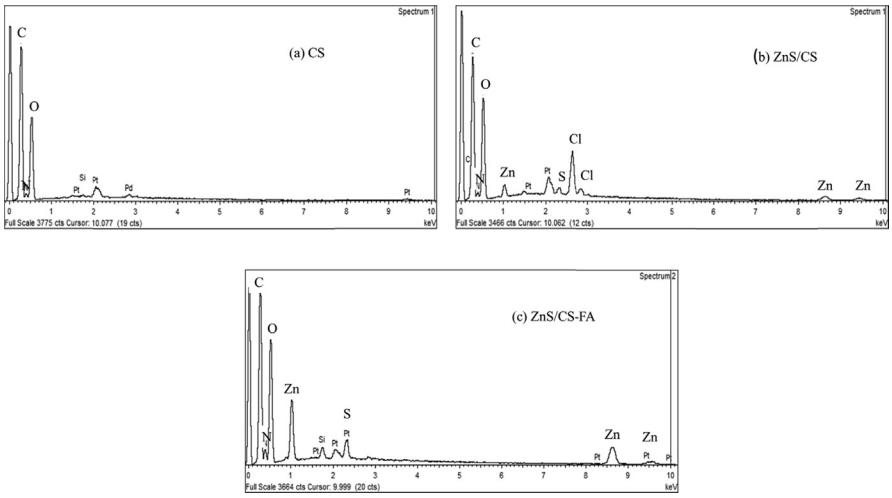

Fig. 7. EDS of (a) Chitosan, (b) ZnS/Chitosan, (c) ZnS/Chitosan-Folic acid.

from yellow to yellow-orange was observed after the reaction with folic acid, further confirming the formation of the final product.

3.6. Size and zeta potential

The average size of the ZnS/CS-FA sample in 1% acetic acid was found to be 463.67 ± 5.76 nm (Fig. 8), and the polydispersity index (PDI) was 0.29 ± 0.02. The PDI value below 0.300 indicated that the distribution of particle size was in a narrow

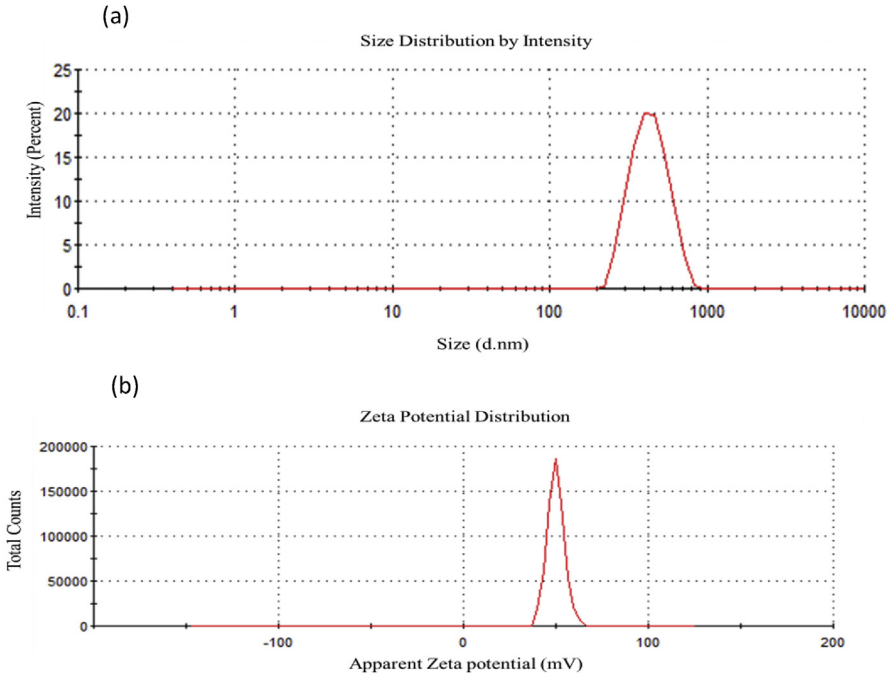

Fig. 8. ZnS/Chitosan-Folic acid nanoparticles (a) average size and polydispersity index, and (b) Zeta potential.

https://doi.org/10.1016/j.heliyon.2018.e00737

range (Ji et al., 2012). The zeta potential (ZP) measurements were carried out for chitosan, ZnS/Chitosan, and ZnS/Chitosan- Folic acid samples dissolved in 1% acetic acid. From the analyzed samples, pure chitosan had a high positive ZP value of 60.06 ± 0.55 mV. This high positive value is expected for the chitosan as its pKa is ~6.5, making it positively charged under acidic conditions. Also, much higher positive ZP values were reported earlier for chitosan under acidic conditions (Bujňáková et al., 2017a). ZnS/Chitosan sample had the ZP value of 58.63 ± 0.93 mV which is close to the values observed before for similar samples (Bujňáková et al., 2017a). Also, it is worth noting that ZP of ZnS/CS is much higher than that of ZnS alone (~19 mV), indicating that these nanoparticles are more stable in the presence of chitosan (Bujňáková et al., 2017a). Then, the ZP of ZnS/CS-FA was measured to be 49.57 ± 1.62 mV. The decrease in ZP after the incorporation of folic acid into the chitosan matrix was also seen in the literature (Yang et al., 2010). This reduction in ZP can be caused due to interactions of folic acid with the positively charged groups on the chitosan surface. However, this high positive ZP indicates that the nanoparticles are stable under the given conditions and holds great potential for uptake through the negatively charged cell membrane.

4. Conclusions

Delivery systems have long been studied as a technique to inhibit the growth of undesirable microbes or cancer cells in areas adjacent to healthy cells. Here chitosan was used as the carrier moiety in the delivery system, while folic acid could potentially provide the target bearing entity for folate or folate like receptors. The addition of zinc provides functionality that will further assist in the destruction of defective cells without harming healthy cells. Comparison of the FTIR, ^{13}C NMR and UV-Vis data of the individual components with that of ZnS/CS-FA indicated the formation of the complex. Thermogravimetric analysis of the samples showed that ZnS/CS-FA has considerable stability in the temperature range up to ~450 °C. Furthermore, the results of SEM-EDS showed that the final product contains chitosan, zinc, and folic acid while size measurements indicated that the size of the ZnS/CS-FA complex is on the nanometer scale.

In the future studies, this ZnS/CS-FA complex will be used in in-vitro studies with cancer cell lines that are known to express folic acid receptors. In these experiments, the solubility of the compound at physiological pH as well as at the pH surrounding the tumor cell has to be considered. Also, it will be required to analyze the effective concentration of the complex that is needed to provide the required apoptotic effect while releasing the right amount of Zn at the target site. Furthermore, the stability of the final product has to be considered in order to evaluate the possible storage conditions and clinical usage.

https://doi.org/10.1016/j.heliyon.2018.e00737

Declarations

Author contribution statement

Subhani Bandara - Performed the experiments; Analyzed and interpreted the data; Wrote the paper.

Codi-anne Carnegie, Chevaun Johnson, Ebonee Williams - Performed the experiments; Analyzed and interpreted the data.

Feyisayo Akindoju, Julia M. Swaby - Analyzed and interpreted the data.

Aderemi Oki - Conceived and designed the experiments; Analyzed and interpreted the data.

Laura E. Carson - Conceived and designed the experiments; Analyzed and interpreted the data; Contributed reagents, materials, analysis tools or data; Wrote the paper.

Funding statement

This work was supported by NIH-NIGMS grant # 1SC3GM121229 and Welch Foundation Grant to Chemistry Department, PVAMU.

Competing interest statement

The authors declare no conflict of interest.

Additional information

No additional information is available for this paper.

Acknowledgements

The authors acknowledge Dr. Paul Johnson at PVAMU for his assistance with the figures.

References

Al-Adilee, K.J., Abass, A.K., Taher, A.M., 2016. Synthesis of some transition metal complexes with new heterocyclic thiazolyl azo dye and their uses as sensitizers in photo reactions. J. Mol. Struct. 1108, 378–397.

Bakrudeen, H.B., Sugunalakshmi, M., Reddy, B.S.R., 2015. Auto-fluorescent mesoporous ZnO nanospheres for drug delivery Carrier application. Mater. Sci. Eng. C Mater. Biol. Appl. 56, 335–340.

https://doi.org/10.1016/j.heliyon.2018.e00737

Bujňáková, Z., Dutková, E., Kello, M., Mojzis, J., Balaz, M., Balaz, P., Shpotyuk, O., 2017a. Mechanochemistry of chitosan-coated zinc sulfide (ZnS) nanocrystals for bio-imaging applications. Nanoscale Res. Lett. 12 (1), 328.

Bujňáková, Z., Dutková, E., Zorkovská, A., Baláž, M., Kováč, J., Kello, M., Mojžiš, J., Briančin, J., Baláž, P., 2017b. Mechanochemical synthesis and in vitro studies of chitosan-coated InAs/ZnS mixed nanocrystals. J. Mater. Sci. 52 (2), 721−735.

Bwatanglang, I.B., Mohammad, F., Yusof, N.A., Abdullah, J., Hussein, M.Z., Alitheen, N.B., Abu, N., 2016. Folic acid targeted Mn:ZnS quantum dots for theranostic applications of cancer cell imaging and therapy. Int. J. Nanomed. 11, 413−428.

Carson, L., Kelly-Brown, C., Stewart, M., Oki, A., Regisford, G., Luo, Z.P., Bakhmutov, V.I., 2009. Synthesis and characterization of chitosan-carbon nanotube composites. Mater. Lett. 63 (6-7), 617−620.

Cho, H.S., Dong, Z.Y., Pauletti, G.M., Zhang, J.M., Xu, H., Gu, H.C., Wang, L.M., Ewing, R.C., Huth, C., Wang, F., Shi, D.L., 2010. Fluorescent, superparamagnetic nanospheres for drug storage, targeting, and imaging: a multifunctional nanocarrier system for cancer diagnosis and treatment. ACS Nano 4 (9), 5398−5404.

Colangelo, F., Roviello, G., Ricciotti, L., Ferone, C., Cioffi, R., 2013. Preparation and characterization of new geopolymer-epoxy resin hybrid mortars. Materials 6 (7), 2989−3006.

Coleman, J.E., 1992. Zinc proteins: enzymes, storage proteins, transcription factors, and replication proteins. Annu. Rev. Biochem. 61, 897−946.

Crider, K.S., Bailey, L.B., Berry, R.J., 2011. Folic acid food fortification-its history, effect, concerns, and future directions. Nutrients 3 (3), 370−384.

Gan, Q., Wang, T., Cochrane, C., McCarron, P., 2005. Modulation of surface charge, particle size and morphological properties of chitosan-TPP nanoparticles intended for gene delivery. Colloids Surfaces B Biointerfaces 44 (2-3), 65−73.

Ganji, F., Abdekhodaie, M.J., 2008. Synthesis and characterization of a new thermosensitive chitosan−PEG diblock copolymer. Carbohydr. Polym. 74 (3), 435−441.

Ghosh, G., Kanti Naskar, M., Patra, A., Chatterjee, M., 2006. Synthesis and characterization of PVP-encapsulated ZnS nanoparticles. Opt. Mater. 28 (8), 1047−1053.

Hsu, S.-C., Don, T.-M., Chiu, W.-Y., 2002. Free radical degradation of chitosan with potassium persulfate. Polym. Degrad. Stabil. 75 (1), 73−83.

https://doi.org/10.1016/j.heliyon.2018.e00737

Hughes, G.A., 2005. Nanostructure-mediated drug delivery. Nanomed. Nanotechnol. Biol. Med. 1 (1), 22–30.

Ivan'kova, E.M., Dobrovolskaya, I.P., Popryadukhin, P.V., Kryukov, A., Yudin, V.E., Morganti, P., 2016. In-situ cryo-SEM investigation of porous structure formation of chitosan sponges. Polym. Test. 52, 41–45.

Ji, J., Wu, D., Liu, L., Chen, J., Xu, Y., 2012. Preparation, characterization, and in vitro release of folic acid-conjugated chitosan nanoparticles loaded with methotrexate for targeted delivery. Polym. Bull. 68 (6), 1707–1720.

Joshi, R., Adhikari, S., Patro, B.S., Chattopadhyay, S., Mukherjee, T., 2001. Free radical scavenging behavior of folic acid: evidence for possible antioxidant activity. Free Radic. Biol. Med. 30 (12), 1390–1399.

Khoza, P., Nyokong, T., 2015. Photocatalytic behaviour of zinc tetraamino phthalocyanine-silver nanoparticles immobilized on chitosan beads. J. Mol. Catal. Chem. 399, 25–32.

Li, Q., Dunn, E.T., Grandmaison, E.W., Goosen, M.F.A., 1992. Applications and properties of chitosan. J. Bioact. Compat. Polym. 7 (4), 370–397.

Liu, J., Guo, T.F., Shi, Y.J., Yang, Y., 2001. Solvation induced morphological effects on the polymer/metal contacts. J. Appl. Phys. 89 (7), 3668–3673.

Luong, D., Kesharwani, P., Alsaab, H.O., Sau, S., Padhye, S., Sarkar, F.H., Iyer, A.K., 2017. Folic acid conjugated polymeric micelles loaded with a curcumin difluorinated analog for targeting cervical and ovarian cancers. Colloids Surfaces B Biointerfaces 157, 490–502.

Lv, Y., Li, K., Li, Y.P., 2013. Surface modification of quantum dots and magnetic nanoparticles with PEG-conjugated chitosan derivatives for biological applications. Chem. Pap. 67 (11), 1404–1413.

Mansouri, S., Cuie, Y., Winnik, F., Shi, Q., Lavigne, P., Benderdour, M., Beaumont, E., Fernandes, J.C., 2006. Characterization of folate-chitosan-DNA nanoparticles for gene therapy. Biomaterials 27 (9), 2060–2065.

Mende, M., Schwarz, D., Steinbach, C., Boldt, R., Schwarz, S., 2016. Simultaneous adsorption of heavy metal ions and anions from aqueous solutions on chitosan Investigated by spectrophotometry and SEM-EDX analysis. Colloid. Surface. Physicochem. Eng. Aspect. 510, 275–282.

Ndagi, U., Mhlongo, N., Soliman, M.E., 2017. Metal complexes in cancer therapy - an update from drug design perspective. Drug Des. Dev. Ther. 11, 599–616.

 https://doi.org/10.1016/j.heliyon.2018.e00737

Nickerson, W.J., Webb, M., 1956. Effect of folic acid analogues on growth and cell division of nonexacting microorganisms. J. Bacteriol. 71 (2), 129–139.

Park, J.H., Saravanakumar, G., Kim, K., Kwon, I.C., 2010. Targeted delivery of low molecular drugs using chitosan and its derivatives. Adv. Drug Deliv. Rev. 62 (1), 28–41.

Parveen, S., Misra, R., Sahoo, S.K., 2012. Nanoparticles: a boon to drug delivery, therapeutics, diagnostics and imaging. Nanomed. Nanotechnol. Biol. Med. 8 (2), 147–166.

Plaetzer, K., Krammer, B., Berlanda, J., Berr, F., Kiesslich, T., 2009. Photophysics and photochemistry of photodynamic therapy: fundamental aspects. Laser Med. Sci. 24 (2), 259–268.

Prabaharan, M., 2008. Chitosan derivatives as promising materials for controlled drug delivery. J. Biomater. Appl. 23 (1), 5–36.

Pujana, M.A., Perez-Alvarez, L., Iturbe, L.C., Katime, I., 2014. pH-sensitive chitosan-folate nanogels crosslinked with biocompatible dicarboxylic acids. Eur. Polym. J. 61, 215–225.

Ribeiro, M.V.M., Melo, I.S., Lopes, F.C.C., Moita, G.C., 2016. Development and validation of a method for the determination of folic acid in different pharmaceutical formulations using derivative spectrophotometry, 52, 741–750.

Ryu, S.R., Noda, I., Jung, Y.M., 2010. What is the origin of positional fluctuation of spectral features: true frequency shift or relative intensity changes of two overlapped bands? Appl. Spectrosc. 64 (9), 1017–1021.

Saito, H., Tabeta, R., Ogawa, K., 1987. High-resolution solid-state carbon-13 NMR study of chitosan and its salts with acids: conformational characterization of polymorphs and helical structures as viewed from the conformation-dependent carbon-13 chemical shifts. Macromolecules 20 (10), 2424–2430.

Singh, R., Lillard, J.W., 2009. Nanoparticle-based targeted drug delivery. Exp. Mol. Pathol. 86 (3), 215–223.

Vaezifar, S., Razavi, S., Golozar, M.A., Karbasi, S., Morshed, M., Kamali, M., 2013. Effects of some parameters on particle size distribution of chitosan nanoparticles prepared by ionic gelation method. J. Cluster Sci. 24 (3), 891–903.

Vimala, K., Shanthi, K., Sundarraj, S., Kannan, S., 2017. Synergistic effect of chemo-photothermal for breast cancer therapy using folic acid (FA) modified zinc oxide nanosheet. J. Colloid Interface Sci. 488, 92–108.

 https://doi.org/10.1016/j.heliyon.2018.e00737

Xiao, Y.B., Lin, Z.T., Chen, Y.M., Wang, H., Deng, Y.L., Le, D.E., Bin, J.G., Li, M.Y., Liao, Y.L., Liu, Y.L., Jiang, G.B., Bin, J.P., 2015. High molecular weight chitosan derivative polymeric micelles encapsulating superparamagnetic iron oxide for tumor-targeted magnetic resonance imaging. Int. J. Nanomed. 10, 1155−1172.

Yang, S.J., Lin, F.H., Tsai, K.C., Wei, M.F., Tsai, H.M., Wong, J.M., Shieh, M.J., 2010. Folic acid-conjugated chitosan nanoparticles enhanced protoporphyrin IX accumulation in colorectal cancer cells. Bioconjugate Chem. 21 (4), 679−689.

https://doi.org/10.1016/j.heliyon.2018.e00737